Radiative corrections to W-boson hadroproduction: higher-order electroweak and supersymmetric effects

SILJA BRENSING[1], STEFAN DITTMAIER[2,3], MICHAEL KRÄMER[1], ALEXANDER MÜCK[1,4]

[1] *Institut für Theoretische Physik E, RWTH Aachen,*
D-52056 Aachen, Germany

[2] *Max-Planck-Institut für Physik (Werner-Heisenberg-Institut),*
D-80805 München, Germany

[3] *Faculty of Physics, University of Vienna,*
A-1090 Vienna, Austria

[4] *Paul Scherrer Institut, Würenlingen und Villigen,*
Ch-5232 Villigen PSI, Switzerland

Abstract:

The high accuracy envisaged for future measurements of W-boson production at hadron colliders has to be matched by precise theoretical predictions. We study the impact of electroweak radiative corrections on W-boson production cross sections and differential distributions at the Tevatron and at the LHC. In particular, we include photon-induced processes, which contribute at $\mathcal{O}(\alpha)$, and leading radiative corrections beyond $\mathcal{O}(\alpha)$ in the high-energy Sudakov regime and from multi-photon final-state radiation. We furthermore present the calculation of the complete supersymmetric next-to-leading-order electroweak and QCD corrections to W-boson hadroproduction within the MSSM. The supersymmetric corrections turn out to be negligible in the vicinity of the W resonance in general, reaching the percent level only at high lepton transverse momentum and for specific choices of the supersymmetric parameters.

1 Introduction

The Drell–Yan-like production of W bosons,

$$pp/p\bar{p} \to W \to l\nu_l X, \tag{1.1}$$

is one of the cleanest hadron collider processes with a large cross section at the Tevatron and at the LHC. Measurements near the W resonance allow for a precise determination of the W-boson mass and yield valuable information on the parton structure of the proton. Above resonance, the off-shell and high-energy tails of appropriate distributions are sensitive to the W width and offer the possibility to search for additional charged gauge bosons W′. (See e.g. Refs. [1, 2] and references therein.)

The high experimental precision envisaged at the Tevatron Run II and specifically at the LHC has to be matched by precise theoretical predictions including QCD and electroweak radiative corrections. The QCD corrections are completely known up to next-to-next-to-leading order (NNLO) [3] and up to N^{3}LO in the soft-plus-virtual approximation [4], with a remaining theoretical error for inclusive cross sections at the percent level or lower. The next-to-leading-order (NLO) QCD corrections have been matched with parton showers [5] and combined with a summation of soft gluon radiation (see e.g. Ref. [6]), which is particularly important to reliably predict the W transverse-momentum distribution. A theoretical study of the QCD uncertainties in the determination of the W cross section at hadron colliders has been presented in Ref. [7].

In this article we mainly focus on the electroweak corrections. Given, for example, the anticipated experimental accuracy in the W-boson mass measurement of $10-20\,\mathrm{MeV}$ at the LHC, the inclusion of electroweak corrections beyond final-state radiation is mandatory as their omission would induce a systematic error in the M_{W} determination of $\mathcal{O}(10~\mathrm{MeV})$ (see e.g. Ref. [1]). The complete NLO $\mathcal{O}(\alpha)$ corrections to the parton process $q\bar{q}' \to W \to l\nu_l$ have been calculated by several groups [8–11]. A tuned comparison of cross sections and differential distributions has shown good agreement between the various calculations [1, 12]. Photon-induced processes $\gamma q \to l\nu_l q'$, which also contribute at $\mathcal{O}(\alpha)$, have been computed recently in Refs. [13, 14]. The particular importance of final-state photon radiation for the W-boson mass determination demands a treatment that goes beyond $\mathcal{O}(\alpha)$. Such multi-photon effects have been studied in Refs. [15, 16] and matched to the NLO $\mathcal{O}(\alpha)$ calculation in Ref. [11]. First steps towards combining QCD and electroweak higher-order effects have been taken in Ref. [17]. We note that the $\mathcal{O}(\alpha)$ corrections to hadronic production of on-shell W bosons at large transverse momenta, $pp/p\bar{p} \to W + \mathrm{jet}$, have recently been presented in Ref. [18] for the SM and in Ref. [19] in the MSSM. For related work on electroweak corrections to Z-boson hadroproduction we refer to Refs. [1, 12] and further references therein.

In this paper we improve on our previous $\mathcal{O}(\alpha)$ calculation [9] for $pp/p\bar{p} \to W \to l\nu_l X$ by including photon-induced processes and multi-photon final-state radiation in the structure-function approach. We also discuss the impact of leading electroweak effects beyond $\mathcal{O}(\alpha)$, specifically the Sudakov logarithms that arise in the high-energy regime, and present the calculation of the complete supersymmetric $\mathcal{O}(\alpha)$ electroweak and $\mathcal{O}(\alpha_{\mathrm{s}})$ strong corrections within the minimal supersymmetric Standard Model (MSSM). The purpose of the MSSM calculation is to establish that the impact of virtual supersymmetric particles on the cross section prediction is small and does not spoil the status of single-W-boson production as one of the cleanest Standard Model (SM) candles at hadron colliders.

The paper is organized as follows. In Sect. 2 we describe the inclusion of leading electroweak effects beyond $\mathcal{O}(\alpha)$, the calculation of the photon-induced processes, and the summation of multiple emission of collinear photons off the final-state lepton. Numerical results for W-boson

production at the Tevatron and the LHC including the complete $\mathcal{O}(\alpha)$ and $\mathcal{O}(\alpha_{\mathrm{s}})$ NLO corrections and the higher-order Sudakov and photon radiation effects are presented in Section 2.5. In Section 3 we describe the calculation of the MSSM corrections and discuss their numerical impact on the W cross section and distributions. We conclude in Section 4. Finally, the Appendix provides details on the scenarios of the supersymmetric models under consideration.

2 Higher-order electroweak effects

The calculation of the complete $\mathcal{O}(\alpha)$ corrections to the parton process $q\bar{q}' \to \mathrm{W} \to l\nu_l$ has been described in detail in Ref. [9]. To control the soft and collinear divergences we have used the dipole subtraction method [20]. In this work we employ an extension of the subtraction formalism [21] which allows to calculate cross sections for bare leptons, i.e. cross sections defined without any photon recombination. (For bare final-state leptons, cross sections are not collinear safe in general and will involve logarithms of the charged lepton masses if, for example, lepton identification cuts are applied.) An additional check of the phase-space integration has been performed using phase-space slicing methods as described in Ref. [9].

In the next sections, we present those parts of the calculation that are new and that have not been discussed in Ref. [9]. We present our results for the specific case of W^+ production, $\mathrm{pp/p\bar{p}} \to \mathrm{W}^+ \to l^+\nu_l X$.

2.1 Leading electroweak effects and choice of couplings

In Ref. [9] (Section 2.2) three different input-parameter schemes have been specified for the choice of the electromagnetic coupling constant α that is taken as SM input together with the particle masses. According to the choice of α, the schemes are called "$\alpha(0)$", "$\alpha(M_{\mathrm{Z}}^2)$", and "G_μ" schemes, where α is set to $\alpha_{G_\mu} = \sqrt{2}G_\mu M_{\mathrm{W}}^2(1 - M_{\mathrm{W}}^2/M_{\mathrm{Z}}^2)/\pi$ in the G_μ scheme. As described in Ref. [9], the relative corrections in the various schemes differ by constant contributions proportional to $\Delta\alpha(M_{\mathrm{Z}}^2) \approx 6\%$ and $\Delta r \approx 3\%$, which quantify the running of the electromagnetic coupling from $Q^2 = 0$ to $Q^2 = M_{\mathrm{Z}}^2$ for $\alpha(M_{\mathrm{Z}}^2)$ and the radiative corrections to muon decay for the G_μ scheme, respectively. The bulk of Δr is contained in $\Delta\alpha(M_{\mathrm{Z}}^2) - c_{\mathrm{W}}^2\Delta\rho/s_{\mathrm{W}}^2$, where $\Delta\rho \approx 1\%$ is the universal correction $\propto G_\mu m_{\mathrm{t}}^2$ to the ρ parameter.

The G_μ scheme is distinguished from the two other schemes because the corrections to charged-current four-fermion processes do not contain large contributions from $\Delta\alpha(M_{\mathrm{Z}}^2)$ or $\Delta\rho$ anymore, i.e. these universal renormalization effects are completely absorbed into the leading-order (LO) amplitude. For the $\mathcal{O}(\alpha)$ corrections this property has already been pointed out in Ref. [9], but it also holds at $\mathcal{O}(\alpha^2)$. More precisely, in the G_μ scheme no contributions proportional to $\Delta\alpha(M_{\mathrm{Z}}^2)^n$ (for any positive integer n), proportional to $\Delta\alpha(M_{\mathrm{Z}}^2)\Delta\rho$, and proportional to $\Delta\rho^2$ appear. Based on the arguments given in Ref. [23] this feature was explicitly worked out in Ref. [24] (Section 3) for the related process of charged-current neutrino deep-inelastic scattering; these results obviously apply also to charged-current Drell–Yan scattering via crossing symmetry.

Before concluding that the theoretical uncertainties in the G_μ scheme from missing corrections beyond $\mathcal{O}(\alpha)$ are smaller than in the two other schemes, we shall inspect other known universal dominant corrections at $\mathcal{O}(\alpha)$. Besides the renormalization effects discussed above, the dominant $\mathcal{O}(\alpha)$ corrections, up to moderate parton scattering energies, are due to final-state radiation off the charged lepton, at least for bare leptons where the enhancement by the large mass logarithm $\propto \alpha \ln m_l$ is present. The inclusion of these contributions beyond $\mathcal{O}(\alpha)$, which are due to collinear multi-photon emission, is described in Sect. 2.4 below. Here we merely point out that the appropriate coupling constant α entering the relative correction is $\alpha(0)$, because it accounts

for the emission of photons with $Q^2 = 0$. Thus, when adopting an input-parameter scheme other than the $\alpha(0)$ scheme, one should nevertheless use $\alpha(0)$ to multiply the dominating universal lepton-mass logarithms. Our specific implementation of this procedure is described in Sect. 2.4.

At high parton scattering energies and high transverse lepton momenta, electroweak corrections are dominated by soft and/or collinear gauge-boson exchange. The soft effects, known as Sudakov logarithms, induce powers of $\alpha \ln^2(\hat{s}/M_W^2)$, with subleading soft/collinear contributions involving lower powers in the logarithm. In $\mathcal{O}(\alpha)$, these enhanced electroweak effects drive the relative corrections to $\approx -30\%$ at lepton transverse momenta of about $1\,\text{TeV}$ at the LHC [9]. It is therefore desirable to control this kind of corrections beyond $\mathcal{O}(\alpha)$. We elaborate more on this issue in the next section. Here we just point out that among the considered input-parameter schemes the G_μ scheme should be appropriate to fix α for the leading high-energy logarithms, which are of weak origin.

Following the above arguments, we employ the G_μ scheme in this work, modified only by the change of α_{G_μ} to $\alpha(0)$ in the leading part of final-state radiation. This procedure is expected to be most robust with respect to further corrections beyond $\mathcal{O}(\alpha)$.

2.2 Leading weak corrections in the Sudakov regime

For single-W production at large lepton transverse momenta or W transverse masses, the parton kinematics is restricted to the Sudakov regime, characterized by large Mandelstam parameters $\hat{s}$, $|\hat{t}|, |\hat{u}| \gg M_W^2$.[1] The structure of electroweak corrections beyond $\mathcal{O}(\alpha)$ in this high-energy regime has been investigated in some detail by several groups in recent years (see e.g. Refs. [25–32] and references therein).

As described for example in Refs. [30, 32], the leading electroweak logarithmic corrections, which are enhanced by large factors $L = \ln(\hat{s}/M_W^2)$, can be divided into an SU(2)×U(1)-symmetric part, an electromagnetic part, and a subleading part induced by the mass difference between W and Z bosons. The last part does not contribute to corrections $\propto (\alpha L^2)^n$ and is neglected in the following. The leading (Sudakov) logarithms $\propto (\alpha L^2)^n$ of electromagnetic origin cancel between virtual and real (soft) bremsstrahlung corrections; for the subleading logarithms such cancellations should strongly depend on the observable under consideration. The only source of leading logarithms is, thus, the symmetric electroweak (sew) part, which can be characterized by comprising W bosons, Z bosons, and photons of a common mass M_W. Using this mass assignment, the one-loop correction $\delta_{\text{sew}}^{(1)}$ to the squared amplitude can be obtained by expanding the full result for the virtual correction δ^{virt} (given in Appendix A of Ref. [9]) for large $\hat{s}, |\hat{t}|, |\hat{u}| \gg M_W^2$. The explicit result can be written as

$$\delta_{\text{sew}}^{(1)} = \frac{\alpha}{2\pi} \left\{ -L^2 C_{1,\text{CC}}^{\text{sew}} + L C_{1,\text{CC}}^{\text{ad}} \right\} \tag{2.1}$$

with factors

$$C_{1,\text{CC}}^{\text{sew}} = \frac{3}{2s_W^2} + \frac{Y_{u_L}^2 + Y_{\nu_{l,L}}^2}{4c_W^2}, \qquad C_{1,\text{CC}}^{\text{ad}} = -\frac{2}{s_W^2}\left[\ln\left(\frac{-\hat{t}}{\hat{s}}\right) + \ln\left(\frac{-\hat{u}}{\hat{s}}\right)\right] + \frac{2}{c_W^2} Y_{u_L} Y_{\nu_{l,L}} \ln\left(\frac{\hat{u}}{\hat{t}}\right), \tag{2.2}$$

which have been introduced in Section 8.4.2 of Ref. [32]. Here $Y_{u_L} = 1/3$ and $Y_{\nu_{l,L}} = -1$ are the weak hypercharges of the corresponding left-handed particles. In Eq. (2.1) we did not only include the leading Sudakov logarithms $\propto \alpha L^2$, but also the related "angular-dependent" contributions $\propto \alpha L \ln(-\hat{t}/\hat{s})$ or $\alpha L \ln(-\hat{u}/\hat{s})$. Our explicit $\mathcal{O}(\alpha)$ result is in agreement with the

---

[1]We use the same notation for the kinematical variables as defined in Ref. [9].

general results presented in Refs. [30, 32], where the corresponding corrections are also given at the two-loop level. These $\mathcal{O}(\alpha^2)$ corrections can be obtained from the $\mathcal{O}(\alpha)$ result by an appropriate exponentiation [28]. For the leading "sew" corrections (including $\alpha^2 L^4$, $\alpha^2 L^3 \ln(-\hat{t}/\hat{s})$, and $\alpha^2 L^3 \ln(-\hat{u}/\hat{s})$ terms) this exponentiation simply reads [32]

$$|\mathcal{M}|^2 \sim |\mathcal{M}_0|^2 \exp\left\{\delta_{\text{sew}}^{(1)}\right\} = |\mathcal{M}_0|^2 \left(1 + \delta_{\text{sew}}^{(1)} + \delta_{\text{sew}}^{(2)} + \dots\right) \tag{2.3}$$

with

$$\delta_{\text{sew}}^{(2)} = \left(\frac{\alpha}{2\pi}\right)^2 \left\{\frac{1}{2}L^4 (C_{1,\text{CC}}^{\text{sew}})^2 - L^3 C_{1,\text{CC}}^{\text{sew}} C_{1,\text{CC}}^{\text{ad}}\right\}. \tag{2.4}$$

However, in the case of neutral-current-induced fermion–antifermion scattering processes it was observed [31] that large cancellations take place between leading and subleading logarithms. In view of this uncertainty, we do not include the two-loop high-energy logarithms in our full predictions. Instead, we evaluate the leading two-loop part $\delta_{\text{sew}}^{(2)}$ as a measure of missing electroweak corrections beyond $\mathcal{O}(\alpha)$ in the high-energy Sudakov regime.

Moreover, since the electroweak high-energy logarithmic corrections are associated with virtual soft and/or collinear weak-boson or photon exchange, they all have counterparts in real weak-boson or photon emission processes which can partially cancel (but not completely, see Ref. [26]) the large negative corrections. To which extent the cancellation occurs depends on the experimental possibilities to separate final states with or without weak bosons or photons. This issue is discussed for example in Ref. [33].

2.3 Photon-induced processes

The $\mathcal{O}(\alpha)$ corrections to the parton cross section $q\bar{q}' \to \text{W}^+ \to l^+\nu_l$ contain collinear singularities from photon radiation off the initial-state quarks which are absorbed by mass factorization [9–11]. For a complete and theoretically consistent analysis, the absorption of the $\mathcal{O}(\alpha)$ collinear singularities into quark distributions has to be complemented by both the inclusion of $\mathcal{O}(\alpha)$ corrections to the parton distribution functions (PDFs) and by the inclusion of the $\mathcal{O}(\alpha)$ partonic subprocesses $\gamma\,\text{u} \to l^+\nu_l\text{d}$ and $\gamma\,\bar{\text{d}} \to l^+\nu_l\bar{\text{u}}$, which were first calculated in Ref. [13]. At the time of our previous study [9] a complete analysis of $\mathcal{O}(\alpha)$ corrections to PDFs, which involves $\mathcal{O}(\alpha)$ corrections to the DGLAP evolution and to the fit of experimental data, was not available. Meanwhile, the MRSTQED2004 [34] PDF parametrization, however, includes these $\mathcal{O}(\alpha)$ corrections and provides a photon density within protons and antiprotons. It is thus now possible to perform a complete $\mathcal{O}(\alpha)$ analysis and to properly include the photon-induced subprocesses in the hadronic cross-section prediction.

The collinear photon splitting into two massless quarks in the subprocesses $\gamma\,\text{u} \to l^+\nu_l\text{d}$ and $\gamma\,\bar{\text{d}} \to l^+\nu_l\bar{\text{u}}$ also leads to a mass singularity. As usual, this divergence is removed by mass factorization. Including both the divergences from collinear photon splitting and the divergence due to collinear photon emission from initial-state quarks in $q\bar{q}' \to l^+\nu_l\gamma$, mass factorization implies a redefinition of the quark densities according to [24]

$$\begin{aligned}
f_q(x) \to f_q(x, \mu_F) &- \int_x^1 \frac{dz}{z}\, f_q\left(\frac{x}{z}, \mu_F\right) Q_q^2 \frac{\alpha}{2\pi} \\
&\times \left\{\ln\left(\frac{\mu_F^2}{m_q^2}\right)\left[P_{qq}(z)\right]_+ - \left[P_{qq}(z)\left(2\ln(1-z)+1\right)\right]_+ + C_{qq}(z)\right\} \\
&- \int_x^1 \frac{dz}{z}\, f_\gamma\left(\frac{x}{z}, \mu_F\right) 3\,Q_q^2 \frac{\alpha}{2\pi}\left\{\ln\left(\frac{\mu_F^2}{m_q^2}\right) P_{q\gamma}(z) + C_{q\gamma}(z)\right\},
\end{aligned} \tag{2.5}$$

4

where Q_q is the electric quark charge, m_q is the small quark mass used as a regulator, and μ_F denotes the QED factorization scale which is identified with the QCD factorization scale. The factor 3 in the second line stems from the splitting of the photon into $q\bar{q}$ pairs of different color. Furthermore,

$$P_{qq}(z) = \frac{1+z^2}{1-z}, \qquad P_{q\gamma}(z) = z^2 + (1-z)^2 \tag{2.6}$$

are the quark and photon splitting functions, respectively, and C_{qq}, $C_{q\gamma}$ the coefficient functions specifying the factorization scheme. Following standard QCD terminology one distinguishes $\overline{\text{MS}}$ and DIS schemes defined by

$$
\begin{aligned}
C_{qq}^{\overline{\text{MS}}}(z) &= C_{q\gamma}^{\overline{\text{MS}}}(z) = 0, \\
C_{qq}^{\text{DIS}}(z) &= \left[P_{qq}(z) \left(\ln \frac{1-z}{z} - \frac{3}{4} \right) + \frac{9+5z}{4} \right]_+, \\
C_{q\gamma}^{\text{DIS}}(z) &= P_{q\gamma}(z) \ln \frac{1-z}{z} - 8z^2 + 8z - 1 \ .
\end{aligned}
\tag{2.7}
$$

In our numerical analysis we employ the MRSTQED2004 parton distribution functions. Note that photon radiation off incoming quarks was ignored in the F_2 fit to HERA data in the MRSTQED2004 PDF determination. Therefore, the MRSTQED2004 PDFs are defined in the DIS scheme for the factorization of QED effects, i.e. *not* in the $\overline{\text{MS}}$ scheme as frequently done in the past (see also Ref. [24]). For the factorization of QCD effects the parton distribution functions are defined in the $\overline{\text{MS}}$ scheme as usual.

To extract the collinear divergence from the squared matrix element for the photon-induced processes we use an extension [21, 24] of the dipole subtraction technique, which has been formulated to treat the collinear splitting of photons into light fermions $\gamma \to f\bar{f}$.

2.4 Multi-photon final-state radiation

The emission of photons collinear to the outgoing charged lepton leads to corrections that are enhanced by large logarithms of the form $\alpha \ln(m_l^2/Q^2)$ with Q denoting a characteristic scale of the process. The KLN theorem [35] guarantees that these logarithms cancel if photons collinear to the lepton are treated fully inclusively. However, since we apply a phase-space cut on the momentum of the outgoing lepton, contributions enhanced by these logarithms survive if the momentum of the bare lepton is considered, i.e. if no photon recombination is performed. While the concept of a bare lepton is not realistic for electrons, it is phenomenologically relevant for muon final states.

The first-order logarithm $\alpha \ln(m_l^2/Q^2)$ is, of course, contained in the full $\mathcal{O}(\alpha)$ correction, so that Q is unambiguously fixed in this order. However, it is desirable to control the logarithmically enhanced corrections beyond $\mathcal{O}(\alpha)$. This can be done in the so-called structure-function approach [36], where these logarithms are derived from the universal factorization of the related mass singularity. The incorporation of the mass-singular logarithms takes the form of a convolution integral over the LO cross section σ_0,

$$\sigma_{\text{LLFSR}} = \int d\sigma_0(p_{\text{u}}, p_{\text{d}}; k_{\nu_l}, k_l) \int_0^1 dz \, \Gamma_{ll}^{\text{LL}}(z, Q^2) \, \Theta_{\text{cut}}(zk_l), \tag{2.8}$$

where the step function Θ_{cut} is equal to 1 if the event passes the cut on the rescaled lepton momentum zk_l and 0 otherwise. The variable z is the momentum fraction describing the lepton energy loss by collinear photon emission. Note that in contrast to the parton-shower approaches

5

to photon radiation (see e.g. Refs. [11, 15, 16]), the structure-function approach neglects the photon momenta transverse to the lepton momentum.

For the structure function $\Gamma_{ll}^{\mathrm{LL}}(z, Q^2)$ we take into account terms up to $\mathcal{O}(\alpha^3)$ improved by the well-known exponentiation of the soft-photonic parts [36],

$$
\begin{aligned}
\Gamma_{ll}^{\mathrm{LL}}(z, Q^2) = {} & \frac{\exp\left(-\frac{1}{2}\beta_l\gamma_{\mathrm{E}} + \frac{3}{8}\beta_l\right)}{\Gamma\left(1 + \frac{1}{2}\beta_l\right)} \frac{\beta_l}{2}(1-z)^{\frac{\beta_l}{2}-1} - \frac{\beta_l}{4}(1+z) \\
& - \frac{\beta_l^2}{32}\left\{\frac{1+3z^2}{1-z}\ln(z) + 4(1+z)\ln(1-z) + 5 + z\right\} \\
& - \frac{\beta_l^3}{384}\left\{(1+z)\left[6\,\mathrm{Li}_2(z) + 12\ln^2(1-z) - 3\pi^2\right]\right. \\
& \qquad\qquad + \frac{1}{1-z}\left[\frac{3}{2}(1+8z+3z^2)\ln(z) + 6(z+5)(1-z)\ln(1-z)\right. \\
& \qquad\qquad\qquad + 12(1+z^2)\ln(z)\ln(1-z) - \frac{1}{2}(1+7z^2)\ln^2(z) \\
& \qquad\qquad\qquad \left.\left. + \frac{1}{4}(39 - 24z - 15z^2)\right]\right\},
\end{aligned}
\tag{2.9}
$$

with γ_E and $\Gamma(y)$ denoting Euler's constant and the Gamma function, respectively. The large logarithm is contained in the variable

$$
\beta_l = \frac{2\alpha(0)}{\pi}\left[\ln\left(\frac{Q^2}{m_l^2}\right) - 1\right].
\tag{2.10}
$$

Here, $\alpha(0)$ is the fine-structure constant defined in the Thomson limit. The parts solely proportional to a power of β_l correspond to collinear (multi-)photon emission off the lepton, the exponential factor describes resummed soft-photonic effects. The non-logarithmic term "-1" in β_l accounts for a non-singular universal soft-photonic correction.

Technically, we add the cross section (2.8) to the one-loop result and subtract the LO and one-loop contributions

$$
\sigma_{\mathrm{LL}^1\mathrm{FSR}} = \int \mathrm{d}\sigma_0(p_{\mathrm{u}}, p_{\mathrm{d}}; k_{\nu_l}, k_l) \int_0^1 \mathrm{d}z\left[\delta(1-z) + \Gamma_{ll}^{\mathrm{LL},1}(z, Q^2)\right]\Theta_{\mathrm{cut}}(zk_l),
\tag{2.11}
$$

contained in (2.8) in order to avoid double counting. The one-loop contribution to the structure function reads

$$
\Gamma_{ll}^{\mathrm{LL},1}(z, Q^2) = \frac{\beta_l}{4}\left(\frac{1+z^2}{1-z}\right)_+.
\tag{2.12}
$$

More precisely, we adapt the value of α in $\Gamma_{ll}^{\mathrm{LL},1}(z, Q^2)$ to the chosen input parameter scheme. Thereby, we introduce an additional higher-order contribution $(\alpha(0) - \alpha)\ln(m_l^2/Q^2)$ so that the $\alpha\ln(m_l^2/Q^2)$ contribution to the full $\mathcal{O}(\alpha)$ correction is subtracted exactly. Hence, the procedure of adding higher-order final-state radiation changes also the value of α in the $\alpha\ln(m_l^2/Q^2)$ term to $\alpha(0)$ which is the appropriate coupling for real-photonic effects.

The uncertainty that is connected with the choice of Q^2 enters in $\mathcal{O}(\alpha^2)$, since all $\mathcal{O}(\alpha)$ corrections, including constant terms, are taken into account. As default we choose the value

$$
Q = \xi\sqrt{\hat{s}}
\tag{2.13}
$$

with $\xi = 1$. In order to quantify the scale uncertainty, we vary ξ between $1/3$ and 3.

6

2.5 Numerical results

2.5.1 Input parameters and setup

The relevant SM input parameters are

$$
\begin{aligned}
G_\mu &= 1.16637 \times 10^{-5}\,\text{GeV}^{-2}, & \alpha(0) &= 1/137.03599911, & \alpha_{\text{s}}(M_Z) &= 0.1189, \\
M_W &= 80.403\,\text{GeV}, & \Gamma_W &= 2.141\,\text{GeV}, \\
M_Z &= 91.1876\,\text{GeV}, & M_H &= 115\,\text{GeV}, \\
m_{\text{e}} &= 0.51099892\,\text{MeV}, & m_\mu &= 105.658369\,\text{MeV}, & m_\tau &= 1.77699\,\text{GeV}, \\
m_{\text{u}} &= 66\,\text{MeV}, & m_{\text{c}} &= 1.2\,\text{GeV}, & m_{\text{t}} &= 174.2\,\text{GeV}, \\
m_{\text{d}} &= 66\,\text{MeV}, & m_{\text{s}} &= 150\,\text{MeV}, & m_{\text{b}} &= 4.6\,\text{GeV}, \\
|V_{\text{ud}}| &= 0.974, & |V_{\text{us}}| &= 0.227, \\
|V_{\text{cd}}| &= 0.227, & |V_{\text{cs}}| &= 0.974, & & & (2.14)
\end{aligned}
$$

which essentially follow Ref. [37]. The masses of the light quarks are adjusted to reproduce the hadronic contribution to the photonic vacuum polarization of Ref. [38]. The CKM matrix is included via global factors in the partonic cross sections for the different initial-state quark flavours. Within loops the CKM matrix is set to unity.

As explained in Sect. 2.1, we adopt the G_μ scheme (up to the modification of α in the final-state radiation), where the electromagnetic coupling α is set to α_{G_μ}. The charge renormalization constant, which contains logarithms of the fermion masses, drops out in the G_μ scheme so that our results are practically independent of the light-quark masses. We keep finite light-quark masses in closed fermion loops, their numerical impact is however extremely small. The W-boson resonance is treated with a fixed width without any running effects.

The $\mathcal{O}(\alpha)$-improved MRSTQED2004 set of PDFs [34] is used throughout. The QCD and QED factorization scales are identified and set to the W-boson mass M_W.

2.5.2 Phase-space cuts and event selection

For the experimental identification of the process $\text{pp}/\text{p}\bar{\text{p}} \to W^+ \to l^+\nu_l X$ we impose the set of phase-space cuts

$$
p_{\text{T},l} > 25\,\text{GeV}, \qquad p\!\!\!/_{\text{T}} > 25\,\text{GeV}, \qquad |\eta_l| < 2.5, \qquad\qquad (2.15)
$$

where $p_{\text{T},l}$ and η_l are the transverse momentum and the rapidity of the charged lepton l^+, respectively, and $p\!\!\!/_{\text{T}} = p_{\text{T},\nu_l}$ is the missing transverse momentum carried away by the neutrino. Note that compared to our previous study [9] we have changed the η_l-cut to $|\eta_l| < 2.5$, which is a more realistic estimate of the experimental charged-lepton coverage at the LHC. The identification cuts are not collinear safe with respect to the lepton momentum, so that observables in general receive corrections that involve large lepton-mass logarithms of the form $\alpha \ln(m_l/M_W)$. This is due to the fact that photons within a small collinear cone around the charged-lepton momentum are not treated inclusively, i.e. the cuts assume a perfect isolation of photons from the charged lepton. While this is (more or less) achievable for muon final states, it is not realistic for electrons. In order to be closer to the experimental situation for electrons, the following photon recombination procedure is applied:

1. Photons with a rapidity $|\eta_\gamma| > 3$, which are close to the beams, are considered part of the proton remnant and are not recombined with the lepton.[2]

2. If the photon survived the first step, and if the resolution $R_{l\gamma} = \sqrt{(\eta_l - \eta_\gamma)^2 + \phi_{l\gamma}^2}$ is smaller than 0.1 (with $\phi_{l\gamma}$ denoting the angle between lepton and photon in the transverse plane), then the photon is recombined with the charged lepton, i.e. the momenta of the photon and of the lepton l are added and associated with the momentum of l, and the photon is discarded.

3. Finally, all events are discarded in which the resulting momentum of the charged lepton does not pass the cuts given in (2.15).

While the electroweak corrections differ for final-state electrons and muons without photon recombination, the corrections become universal in the presence of photon recombination, since the lepton-mass logarithms cancel in this case, in accordance with the KLN theorem. Numerical results are presented for photon recombination and for bare muons.

2.5.3 Cross sections and distributions for $pp \to W^+ \to l^+\nu_l X$ at the LHC

We first consider W^+ production at the LHC, i.e. a pp initial state with a centre-of-mass (CM) energy of $\sqrt{s} = 14\,\mathrm{TeV}$.

In Tables 1 and 2 we present the LO cross section σ_0 and various types of electroweak corrections δ, defined relative to the LO cross section by $\sigma = \sigma_0 \times (1 + \delta)$. The results are shown for different ranges in the transverse momentum of the charged lepton, $p_{\mathrm{T},l}$, and in the transverse mass of the two final-state leptons, $M_{\mathrm{T},\nu_l l} = \sqrt{2 p_{\mathrm{T},l} \not{p}_{\mathrm{T}} (1 - \cos\phi_{\nu_l l})}$, where $\phi_{\nu_l l}$ is the angle between the lepton and the missing momentum in the transverse plane.

For reference, we first update the $\mathcal{O}(\alpha)$ NLO corrections for W-boson hadroproduction through the parton process $q\bar{q}' \to W^+ \to l^+\nu_l$ [9]. The results are given for bare muon final states ($\delta_{q\bar{q}}^{\mu^+\nu_\mu}$) and with photon recombination applied ($\delta_{q\bar{q}}^{\mathrm{rec}}$). As explained above, the mass-singular corrections $\propto \alpha \ln(m_\mu/M_W)$ present in $\delta_{q\bar{q}}^{\mu^+\nu_\mu}$ cancel if the photon is recombined, rendering the corresponding correction $\delta_{q\bar{q}}^{\mathrm{rec}}$ smaller. At large $p_{\mathrm{T},l}$ and $M_{\mathrm{T},\nu_l l}$ the electroweak corrections are dominated by the $\mathcal{O}(\alpha)$ Sudakov logarithms discussed in Sect. 2.2. Note that the relative $\mathcal{O}(\alpha)$ corrections $\delta_{q\bar{q}}$ presented in Tables 1 and 2 are not very sensitive to the choice of the PDF and the choice of the η_l cut and thus agree very well with our previous numerical results presented in Ref. [9].

The $\mathcal{O}(\alpha)$ corrections originating from the photon-induced processes (Sect. 2.3) are not included in $\delta_{q\bar{q}}$, but are shown separately as $\delta_{\gamma q}$ in Tables 1 and 2. They are enhanced at large $p_{\mathrm{T},l}$ because of a new type of contribution where the incoming photon couples to a W boson that is exchanged in the t-channel. The photon-induced processes could in principle be used to extract information on the photon content of the proton. However, they are overwhelmed by QCD corrections and QCD uncertainties which strongly affect the $p_{\mathrm{T},l}$ spectrum (see the discussion of NLO QCD corrections below). If, on the other hand, one considers the distribution in the transverse mass $M_{\mathrm{T},\nu_l l}$, which is much less sensitive to QCD effects, the impact of $\delta_{\gamma q}$ is below the percent level. The results for $\delta_{\gamma q}$ in Tables 1 and 2 are in good agreement with those presented in Refs. [13,14]. Note that in Ref. [14] the mass factorization of the collinear $\gamma \to q\bar{q}$ splitting is

---

[2]Note that collinear safety requires that the $|\eta_\gamma|$ cut must be larger than the lepton identification cut on $|\eta_l|$ to avoid events where an almost collinear lepton–photon pair is not recombined because $|\eta_l| \lesssim 2.5$ and $|\eta_\gamma| \gtrsim 2.5$. It turns out, however, that the numerical difference between choosing $|\eta_\gamma| > 3$ and $|\eta_\gamma| > 2.5$ is negligible.

$$\text{pp} \to l^+\nu_l X \text{ at } \sqrt{s} = 14\,\text{TeV}$$

$p_{\mathrm{T},l}/\mathrm{GeV}$	25–∞	50–∞	100–∞	200–∞	500–∞	1000–∞
σ_0/pb	4495.7(2)	27.589(2)	1.7906(1)	0.18128(1)	0.0065222(4)	0.00027322(1)
$\delta_{q\bar{q}}^{\mu^+\nu_\mu}/\%$	−2.9(1)	−5.1(1)	−8.6(1)	−13.2(1)	−23.4(1)	−34.7(1)
$\delta_{q\bar{q}}^{\mathrm{rec}}/\%$	−1.8(1)	−2.6(1)	−6.1(1)	−10.3(1)	−19.5(1)	−29.5(1)
$\delta_{q\gamma}/\%$	0.065(1)	4.7(1)	12.3(1)	17.1(1)	16.7(1)	13.5(1)
$\delta_{\mathrm{Sudakov}}^{(2)}/\%$	−0.0002	−0.023	−0.082	0.057	1.3	3.8
$\delta_{\mathrm{multi}-\gamma}/\%$	$0.12^{+0.03}_{-0.02}$	$0.31^{+0.08}_{-0.07}$	$0.27^{+0.06}_{-0.05}$	$0.31^{+0.06}_{-0.06}$	$0.41^{+0.08}_{-0.07}$	$0.57^{+0.10}_{-0.09}$
$\delta_{\mathrm{EW}}^{\mu^+\nu_\mu}/\%$	−2.7(1)	0.0(1)	4.0(1)	4.3(1)	−6.3(1)	−20.6(1)
$\delta_{\mathrm{EW}}^{\mathrm{rec}}/\%$	−1.7(1)	2.1(1)	6.2(1)	6.9(1)	−2.7(1)	−16.0(1)
$\delta_{\mathrm{QCD}}^{\mu=M_\mathrm{W}}/\%$	−2.7(1)	812(1)	784(1)	814(1)	611(1)	399(1)
$\delta_{\mathrm{QCD}}^{\mu=M_{\mathrm{T,W}}}/\%$	−2.8(1)	793(1)	685(1)	607(1)	323(1)	127(1)

Table 1: Integrated LO cross sections σ_0 for W^+ production at the LHC for different ranges in $p_{\mathrm{T},l}$ and corresponding relative corrections δ in the SM.

$$\text{pp} \to l^+\nu_l X \text{ at } \sqrt{s} = 14\,\text{TeV}$$

$M_{\mathrm{T},\nu_l l}/\mathrm{GeV}$	50–∞	100–∞	200–∞	500–∞	1000–∞	2000–∞
σ_0/pb	4495.7(2)	27.589(2)	1.7906(1)	0.084697(4)	0.0065222(4)	0.00027322(1)
$\delta_{q\bar{q}}^{\mu^+\nu_\mu}/\%$	−2.9(1)	−5.2(1)	−8.1(1)	−14.8(1)	−22.6(1)	−33.2(1)
$\delta_{q\bar{q}}^{\mathrm{rec}}/\%$	−1.8(1)	−3.5(1)	−6.5(1)	−12.7(1)	−20.0(1)	−29.6(1)
$\delta_{q\gamma}/\%$	0.052(1)	0.12(1)	0.25(1)	0.37(1)	0.39(1)	0.36(1)
$\delta_{\mathrm{Sudakov}}^{(2)}/\%$	−0.0002	−0.023	−0.082	0.21	1.3	3.8
$\delta_{\mathrm{multi}-\gamma}/\%$	$0.12^{+0.03}_{-0.02}$	$0.20^{+0.05}_{-0.04}$	$0.16^{+0.03}_{-0.03}$	$0.19^{+0.04}_{-0.03}$	$0.24^{+0.04}_{-0.04}$	$0.34^{+0.06}_{-0.05}$
$\delta_{\mathrm{EW}}^{\mu^+\nu_\mu}/\%$	−2.7(1)	−4.9(1)	−7.7(1)	−14.2(1)	−22.0(1)	−32.5(1)
$\delta_{\mathrm{EW}}^{\mathrm{rec}}/\%$	−1.7(1)	−3.4(1)	−6.3(1)	−12.3(1)	−19.6(1)	−29.3(1)
$\delta_{\mathrm{QCD}}^{\mu=M_\mathrm{W}}/\%$	−4.2(1)	23.2(1)	26.6(1)	19.1(1)	4.7(1)	−18.5(1)
$\delta_{\mathrm{QCD}}^{\mu=M_{\mathrm{T,W}}}/\%$	−4.4(1)	22.5(1)	24.0(1)	12.6(1)	−6.2(1)	−34.6(1)

Table 2: Integrated LO cross sections σ_0 for W^+ production at the LHC for different ranges in $M_{\mathrm{T},\nu_l l}$ and corresponding relative corrections δ in the SM.

performed in the $\overline{\text{MS}}$ scheme, while the photon distribution of the MRSTQED2004 PDF set is defined in the DIS scheme as argued above. It turns out, however, that the difference between the calculations in the $\overline{\text{MS}}$ and in the DIS scheme is numerically negligible for hadronic cross sections.

We find that the $\mathcal{O}(\alpha^2)$ high-energy Sudakov logarithms calculated in Sect. 2.2, labeled $\delta_{\text{Sudakov}}^{(2)}$ in Tables 1 and 2, have a small impact on the cross-section prediction, below 5% even for a transverse lepton momentum $p_{\text{T},l}$ in the TeV range.

The corrections due to multi-photon final-state radiation beyond $\mathcal{O}(\alpha)$ (see Section 2.4) are shown as $\delta_{\text{multi}-\gamma}$ in the tables. Only the genuine multi-photon effects are included in $\delta_{\text{multi}-\gamma}$, i.e. the one-loop contribution is subtracted. We show $\delta_{\text{multi}-\gamma}$ for the central scale choice $Q = \sqrt{\hat{s}}$ with an uncertainty estimate obtained from varying the scale Q between $Q = 3\sqrt{\hat{s}}$ (upper number) and $Q = \sqrt{\hat{s}}/3$ (lower number). Multi-photon final-state radiation beyond $\mathcal{O}(\alpha)$ has a very small effect on the cross sections displayed in Tables 1 and 2. The largest part of this small contribution is in fact due to the change of the coupling constant α from α_{G_μ} to $\alpha(0)$ in the relative $\mathcal{O}(\alpha)$ correction. However, as we shall discuss below, the contribution from multi-photon final-state radiation reaches the percent level near the W resonance and has thus a significant impact on a precision determination of the W mass. A more detailed analysis is needed to quantify the corresponding shift in the determination of M_{W} (cf. Refs. [1, 15, 39]).

For convenience we combine the above results and display our best estimate for i) the electroweak corrections for muon final states $\delta_{\text{EW}}^{\mu^+\nu_\mu}$, which includes the $\mathcal{O}(\alpha)$ correction to the $q\bar{q}'$ initial states, the corrections due to the photon-induced processes, and the multi-photon final-state radiation corrections with the scale choice $Q = \sqrt{\hat{s}}$, and ii) the total electroweak correction for final states with photon recombination $\delta_{\text{EW}}^{\text{rec}}$, which combines the $\mathcal{O}(\alpha)$ corrections from $q\bar{q}'$ and γq initial states and which is not sensitive to multi-photon final-state radiation. Because of the theoretical uncertainty in evaluating the higher-order weak corrections in the high-energy regime (see the discussion in Sect. 2.2), we do not include the leading two-loop Sudakov logarithms $\delta_{\text{Sudakov}}^{(2)}$ in our best estimate of the electroweak corrections.

For comparison, we have also calculated the NLO QCD corrections, evaluated with two different choices for the renormalization and factorization scales, $\mu_R = \mu_F = M_{\text{W}}$ ($\delta_{\text{QCD}}^{\mu=M_{\text{W}}}$) and $\mu_R = \mu_F = M_{\text{T},\text{W}}$ with $M_{\text{T},\text{W}}^2 = M_{\text{W}}^2 + p_{\text{T},\text{W}}^2$ ($\delta_{\text{QCD}}^{\mu=M_{\text{T},\text{W}}}$), where $p_{\text{T},\text{W}}$ is the transverse momentum of the W boson to be evaluated on an event-by-event basis. We have compared our NLO QCD results for $\delta_{\text{QCD}}^{\mu=M_{\text{W}}}$ with those obtained from MCFM [40] and find good agreement. In the QCD case, there is of course only initial-state radiation and thus no technical need for a recombination procedure of the charged lepton with a possible additional jet. Rather, one should employ a separation cut between lepton and jet to allow for a clean event selection. However, since we only want to give a rough estimate of the size of QCD effects for comparison with the electroweak corrections, for simplicity, we do not include any sort of separation cut. As indicated above, the QCD corrections are extremely large at large $p_{\text{T},l}$ so that the electroweak corrections to the $p_{\text{T},l}$ distribution are overwhelmed by QCD uncertainties. The $M_{\text{T},\nu_l l}$ distribution, on the other hand, is much less sensitive to higher-order QCD effects. It is invariant under transverse boosts to first order in the velocity of the W boson and thus not strongly affected by a transverse momentum of the W boson induced by gluon radiation at NLO QCD [41].

The size of the QCD corrections to the $p_{\text{T},l}$ distribution can be reduced by applying a jet veto. Table 3 shows the impact of a jet veto on the NLO QCD calculation where we restrict the additional parton to a transverse momentum $p_{\text{T},\text{jet}}$ ($= p_{\text{T},\text{W}}$ at NLO) < 50 GeV. Of course, the jet veto also reduces the size of the photon-induced processes as demonstrated in Table 3.

In Figures 1 and 2 we show the differential cross sections and the corresponding corrections with respect to the transverse momentum $p_{\text{T},l}$ and the transverse mass $M_{\text{T},\nu_l l}$, respectively. The
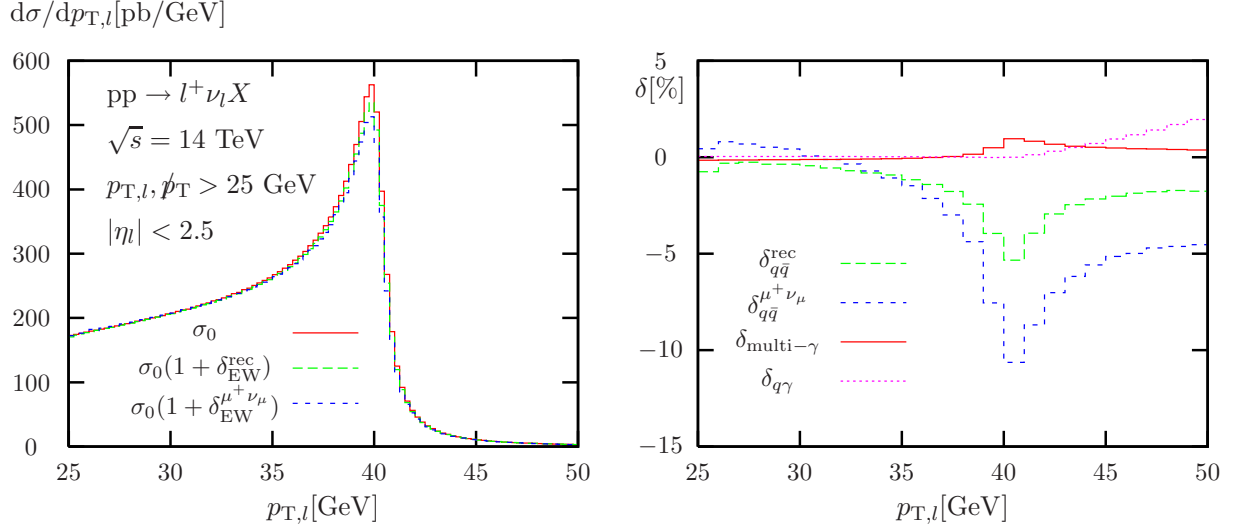
$\mathrm{d}\sigma/\mathrm{d}p_{\mathrm{T},l}[\mathrm{pb/GeV}]$

Figure 1: Lepton-transverse-momentum distribution in LO and corresponding relative corrections δ at the LHC in the SM.

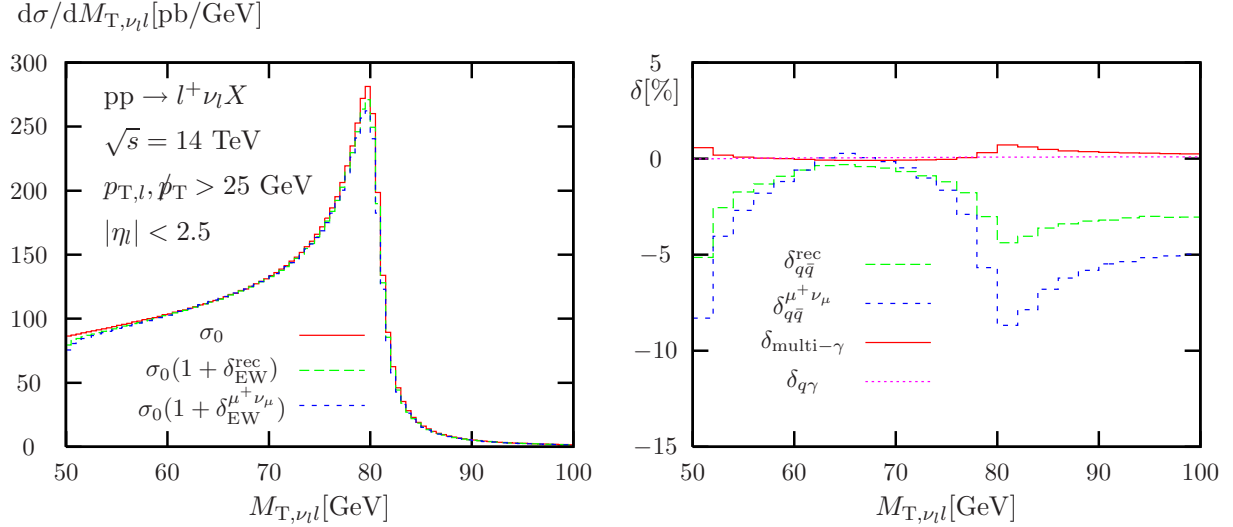$\mathrm{d}\sigma/\mathrm{d}M_{\mathrm{T},\nu_l l}[\mathrm{pb/GeV}]$

Figure 2: W-transverse-mass distribution in LO and corresponding relative corrections δ at the LHC in the SM.

$$\text{pp} \rightarrow l^+ \nu_l X \text{ at } \sqrt{s} = 14\,\text{TeV}$$

$p_{\mathrm{T},l}/\text{GeV}$	25–∞	50–∞	100–∞	200–∞	500–∞	1000–∞
$\delta_{q\gamma,\text{veto}}/\%$	0.025(1)	1.2(1)	0.049(1)	0.043(1)	0.042(1)	0.042(1)
$\delta_{\mathrm{QCD},\text{veto}}^{\mu=M_\mathrm{W}}/\%$	$-7.3(1)$	454(1)	6.4(1)	$-15.8(1)$	$-51.9(1)$	$-85.0(1)$

Table 3: Relative corrections for W^+ production at the LHC from the photon-induced processes and from the NLO QCD calculation with a jet veto imposed. We require the additional parton to be produced at $p_{\mathrm{T,jet}} < 50$ GeV.

distributions show the well-known kinks at $p_{\mathrm{T},l} \approx M_\mathrm{W}/2$ and $M_{\mathrm{T},\nu_l} \approx M_\mathrm{W}$, which are used in the W-mass determination. Near these kinks the correction $\delta_{q\bar{q}}$ reaches the order of 10% for bare muons and is reduced to about 5% after photon recombination. Near the resonance region, the corrections from photon-induced processes are very small. Multi-photon emission, on the other hand, reaches the percent level near $p_{\mathrm{T},l} \approx M_\mathrm{W}/2$ and $M_{\mathrm{T},\nu_l} \approx M_\mathrm{W}$ and induces some distortion that affects the M_W determination from the shape of the M_{T,ν_l} distribution. The two-loop Sudakov corrections are, of course, completely negligible near the W resonance and are thus not displayed in Figures 1 and 2.

2.5.4 Cross sections and distributions for $\text{p}\bar{\text{p}} \rightarrow \mathrm{W}^+ \rightarrow l^+\nu_l X$ at the Tevatron

We also present numerical results for W production at the Tevatron, i.e. a $\text{p}\bar{\text{p}}$ collider with a CM energy of $\sqrt{s} = 1.96\,\text{TeV}$. We again use the phase-space cuts of (2.15) and the photon recombination procedure specified in the previous section.

Tables 4/5 and Figures 3/4 display the LO cross section σ_0 and the various relative corrections δ as a function of the transverse momentum and transverse mass. The electroweak corrections are typically of the same size as those discussed for the LHC, and also show the same qualitative features. It is obvious that the high-energy Sudakov regime is not phenomenologically relevant for W production at the Tevatron, and that the size of the two-loop Sudakov corrections at moderate $p_{\mathrm{T},l}$ and M_{T,ν_l} is no reliable estimate of the theoretical uncertainty from missing electroweak two-loop corrections.

3 Supersymmetric corrections in the MSSM

Non-standard physics could affect the W-boson cross-section prediction and thus bias the precision determination of Standard Model parameters from W-boson observables at hadron colliders. To quantify the impact of new physics on the W cross section in a concrete model, we have calculated the $\mathcal{O}(\alpha)$ electroweak and $\mathcal{O}(\alpha_\mathrm{s})$ strong corrections to $\text{pp/p}\bar{\text{p}} \rightarrow \mathrm{W}^+ \rightarrow l^+\nu_l X$ within the MSSM.

3.1 Supersymmetric QCD and electroweak corrections

The SUSY-QCD corrections comprise gluino–squark loops which contribute to the $q\bar{q}'\mathrm{W}$ vertex correction and to the quark wave-function renormalization.

To obtain the electroweak SUSY corrections, we calculate the complete electroweak $\mathcal{O}(\alpha)$ corrections in the MSSM and subtract the SM corrections, so that the MSSM corrections can be

p$\overline{\text{p}}$ → $l^+\nu_l X$ at $\sqrt{s} = 1.96\,\text{TeV}$

$p_{\text{T},l\nu}$/GeV	25–∞	50–∞	75–∞	100–∞	200–∞	300–∞
σ_0/pb	706.95(1)	3.7496(2)	0.51112(2)	0.152014(6)	0.0056405(2)	0.00039160(2)
$\delta_{q\bar{q}}^{\mu^+\nu_\mu}$/%	−2.7(1)	−5.4(1)	−7.4(1)	−9.1(1)	−14.2(1)	−18.6(1)
$\delta_{q\bar{q}}^{\text{rec}}$/%	−1.7(1)	−2.8(1)	−4.9(1)	−6.3(1)	−10.3(1)	−13.7(1)
$\delta_{q\gamma}$/%	0.020(1)	1.5(1)	2.0(1)	2.0(1)	1.4(1)	0.95(1)
$\delta_{\text{Sudakov}}^{(2)}$/%	−0.0001	−0.017	−0.056	−0.078	−0.013	0.20
$\delta_{\text{multi}-\gamma}$/%	$0.11^{+0.02}_{-0.02}$	$0.34^{+0.09}_{-0.08}$	$0.30^{+0.07}_{-0.06}$	$0.32^{+0.07}_{-0.07}$	$0.45^{+0.09}_{-0.09}$	$0.59^{+0.12}_{-0.11}$
$\delta_{\text{EW}}^{\mu^+\nu_\mu}$/%	−2.6(1)	−3.5(1)	−5.1(1)	−6.8(1)	−12.3(1)	−17.1(1)
$\delta_{\text{EW}}^{\text{rec}}$/%	−1.6(1)	−1.3(1)	−2.9(1)	−4.3(1)	−8.9(1)	−12.8(1)
$\delta_{\text{QCD}}^{\mu=M_W}$/%	11.2(1)	377(1)	205(1)	174(1)	113(1)	74.6(1)
$\delta_{\text{QCD}}^{\mu=M_{\text{T,w}}}$/%	11.0(1)	362(1)	176(1)	138(1)	69.9(1)	34.9(1)

Table 4: Integrated LO cross sections σ_0 for W^+ production at the Tevatron for different ranges in $p_{\text{T},l}$ and corresponding relative corrections δ in the SM.

p$\overline{\text{p}}$ → $l^+\nu_l X$ at $\sqrt{s} = 1.96\,\text{TeV}$

$M_{\text{T},\nu_l l}$/GeV	50–∞	100–∞	150–∞	200–∞	400–∞	600–∞
σ_0/pb	706.95(1)	3.7496(2)	0.51112(2)	0.152014(6)	0.0056405(2)	0.00039160(2)
$\delta_{q\bar{q}}^{\mu^+\nu_\mu}$/%	−2.7(1)	−5.2(1)	−6.5(1)	−8.0(1)	−12.7(1)	−16.8(1)
$\delta_{q\bar{q}}^{\text{rec}}$/%	−1.7(1)	−3.4(1)	−4.8(1)	−6.2(1)	−10.1(1)	−13.3(1)
$\delta_{q\gamma}$/%	0.017(1)	0.028(1)	0.028(1)	0.027(1)	0.018(1)	0.012(1)
$\delta_{\text{Sudakov}}^{(2)}$/%	−0.0001	−0.017	−0.056	−0.078	−0.013	0.20
$\delta_{\text{multi}-\gamma}$/%	$0.11^{+0.02}_{-0.02}$	$0.21^{+0.05}_{-0.05}$	$0.18^{+0.04}_{-0.04}$	$0.19^{+0.04}_{-0.04}$	$0.27^{+0.05}_{-0.05}$	$0.37^{+0.07}_{-0.07}$
$\delta_{\text{EW}}^{\mu^+\nu_\mu}$/%	−2.6(1)	−4.9(1)	−6.3(1)	−7.8(1)	−12.4(1)	−16.4(1)
$\delta_{\text{EW}}^{\text{rec}}$/%	−1.6(1)	−3.4(1)	−4.8(1)	−6.1(1)	−10.0(1)	−13.3(1)
$\delta_{\text{QCD}}^{\mu=M_W}$/%	10.8(1)	22.1(1)	19.6(1)	16.7(1)	6.2(1)	−2.8(1)
$\delta_{\text{QCD}}^{\mu=M_{\text{T,w}}}$/%	10.5(1)	21.4(1)	18.5(1)	15.3(1)	4.1(1)	−5.3(1)

Table 5: Integrated LO cross sections σ_0 for W^+ production at the Tevatron for different ranges in $M_{\text{T},\nu_l l}$ and corresponding relative corrections δ in the SM.
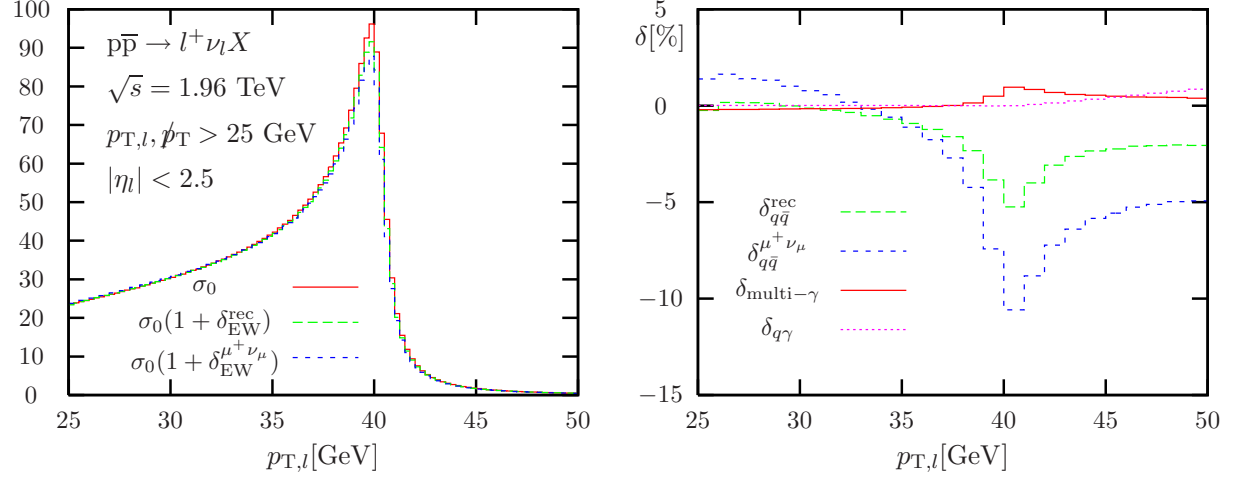
dσ/d$p_{\mathrm{T},l}$[pb/GeV]

Figure 3: Lepton-transverse-momentum distribution in LO and corresponding relative corrections δ at the Tevatron in the SM.

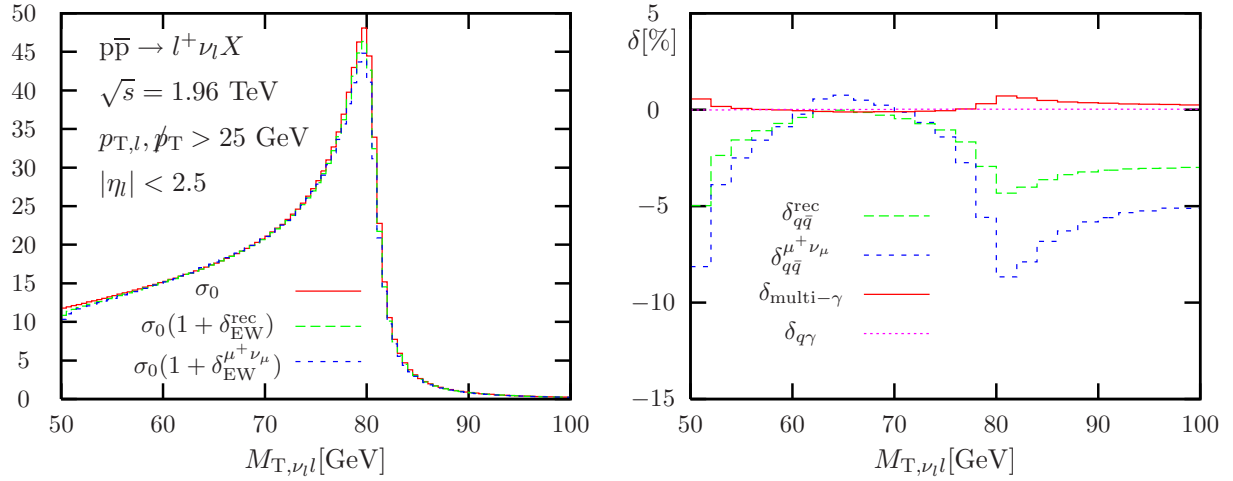dσ/d$M_{\mathrm{T},\nu_l l}$[pb/GeV]

Figure 4: W-transverse-mass distribution in LO and corresponding relative corrections δ at the Tevatron in the SM.
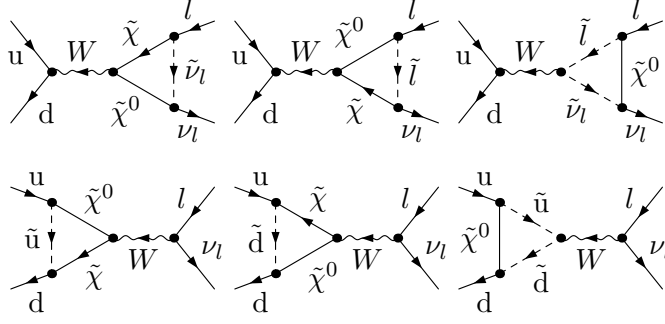
14

Figure 5: Classes of diagrams for the additional vertex corrections within the MSSM. The neutralinos $\tilde{\chi}^0$, charginos $\tilde{\chi}$, squarks $\tilde{q}$ ($q = $ u, d) and sleptons $\tilde{l}$ represent the different possible mass eigenstates.
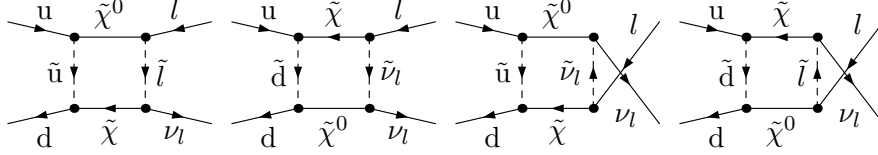

Figure 6: Classes of diagrams for the additional box corrections within the MSSM. The neutralinos $\tilde{\chi}^0$, charginos $\tilde{\chi}$, squarks $\tilde{q}$ ($q = $ u, d) and sleptons $\tilde{l}$ represent the different possible mass eigenstates.

added to the SM predictions of the previous section without double counting. This procedure applies to the vertex, box, and self-energy corrections as well as to the counterterms and Δr. The diagrams for the genuine SUSY vertex and box corrections are shown in Figures 5 and 6, respectively. The subtraction is only non-trivial for contributions from the Higgs sector where the SM and MSSM vertex appears with different couplings. However, for massless external fermions the Higgs sector only contributes to the W-boson self-energy and to renormalization constants. The mass of the lightest MSSM Higgs boson is used as SM input when we subtract the SM contribution to the correction. Hence, for ultimate precision, one would have to calculate the SM corrections with the appropriate Higgs mass.

The diagrammatic calculation is performed in two almost independent ways. Both calculations use FeynArts [42] to generate the relevant (MSSM) diagrams. One of the calculations then employs FormCalc and LoopTools [43] to perform the algebraic calculation and the loop integrals while the other calculation uses a completely independent set of in-house routines for both the algebraic calculation and for the numerical evaluation.

3.2 Numerical results

3.2.1 Input parameters and setup

The SM input parameters and the setup of the calculation (input parameter scheme, PDFs, cuts, etc.) are chosen as described in Sect. 2.5.1.

To study the dependence of the corrections on the SUSY breaking parameters, we show results for all the SPS benchmark scenarios [44]. These benchmarks are valuable, because they cover typical SUSY scenarios in different regions of parameter space, even though most of them are meanwhile excluded by experimental data. The SPS points are defined by the low-energy SUSY breaking parameters which determine the spectrum and the couplings. For the ten benchmark scenarios under consideration in this work, this input [45] is tabulated in Appendix A.

Dependent SUSY parameters, such as Higgs, chargino, neutralino, or sfermion masses, are calculated from the SPS input using tree-level relations. Since the impact of the fermion masses of the first two generations is negligible, these masses are set to zero in the calculation of the corresponding sfermion mass matrices. Following this approach the SUSY corrections do not depend on the fermion generations in the partonic process $u\bar{d} \to l^+ \nu_l$. In particular, the SUSY corrections presented below are valid for both outgoing electrons and muons.

3.2.2 Corrections to partonic cross sections

In order to exhibit the typical features of the SUSY corrections it is instructive to first discuss the inclusive partonic cross section $\hat{\sigma}_0$ evaluated at a fixed partonic CM energy $\sqrt{\hat{s}}$. Here, no cuts are applied. In Figure 7 we display the LO result and the SUSY-EW and SUSY-QCD corrections as a function of the parton energy $\sqrt{\hat{s}}$ for the ten different SPS scenarios.

The SUSY-QCD corrections turn out to be completely negligible for parton energies below $1\,\mathrm{TeV}$, as the SPS scenarios involve heavy squarks and gluinos which effectively decouple. The SUSY-QCD corrections reach the $+1\%$ level only when the sum of the gluino and a squark mass equals $\sqrt{\hat{s}}$, which typically happens between 1 and $2\,\mathrm{TeV}$ for the SPS scenarios. For even larger parton energies well above the squark/gluino mass scale the SUSY-QCD corrections turn negative and become logarithmically enhanced with increasing $\hat{s}$. In Figure 7, the corrections are only shown up to the phenomenologically relevant region $\sqrt{\hat{s}} = 2$ TeV such that the asymptotic behavior is not visible.

The EW corrections turn on at smaller $\sqrt{\hat{s}}$ and exhibit peaks which correspond to sparticle thresholds. Specifically, corrections at the -1% level occur if the sum of a neutralino and a chargino mass equals $\sqrt{\hat{s}}$ and if the sleptons and squarks in the model are heavy compared to this mass scale. The corrections then rise logarithmically with $\hat{s}$ to positive values. At the mass scale of the sleptons and squarks there is an additional negative contribution to the correction which is less peaked than the gaugino peaks and which washes out the gaugino peaks if the corresponding regions overlap.

3.2.3 Corrections to hadronic cross sections

To calculate the hadronic MSSM cross section we apply the same phase-space cuts as for the SM analysis. However, since the MSSM corrections are purely virtual, the kinematics of the relevant events is as in leading order, i.e. photon recombination is irrelevant and $M_{\mathrm{T},\nu_l l} = 2p_{\mathrm{T},l}$. In Table 6, we show the integrated cross section for different ranges in $p_{\mathrm{T},l}$ in analogy to the SM analysis in Section 2.5. As expected, the corrections for relatively low $p_{\mathrm{T},l}$ cuts are negligible at the sub-per-mille level. Only in the high-$p_{\mathrm{T},l}$ tail, the EW corrections reach the percent level if the SUSY spectrum is light enough. This rise in the corrections in the high-$p_{\mathrm{T},l}$ tail depends on the mass scale of the relevant SUSY particles in the loops. The maximum of the corrections is reached for the SPS 2 scenario where the gauginos are particularly light and the squarks and sleptons are so heavy that their negative contribution becomes effective only at even larger $p_{\mathrm{T},l}$.

SPS 2 is also the only scenario for which the EW corrections in the $p_{\mathrm{T},l}$ distribution, as shown in Figure 8, almost reach the percent level for $p_{\mathrm{T},l} < 100$ GeV due to the light gauginos. In the
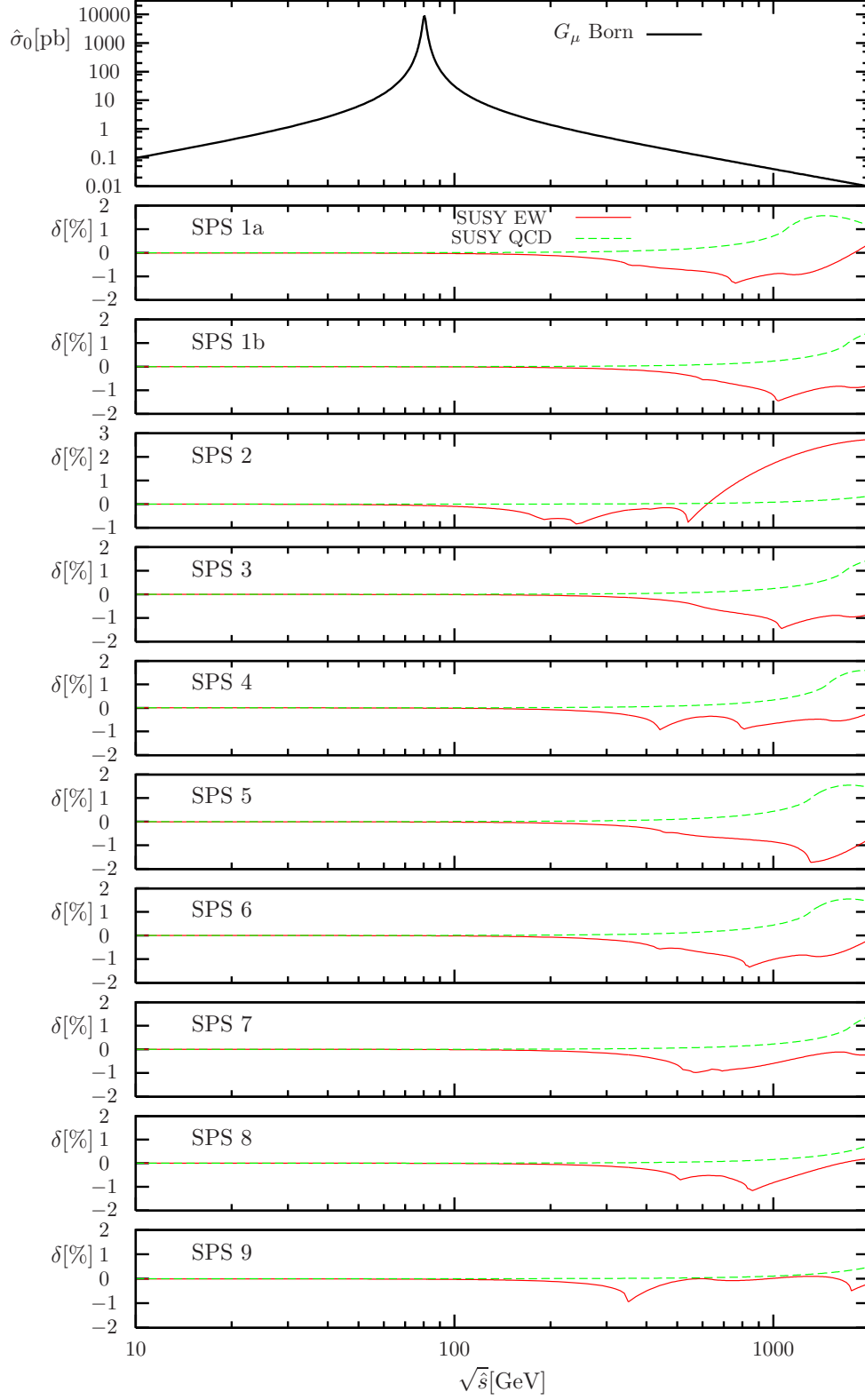
Figure 7: Total partonic LO cross section $\hat{\sigma}_0$ and corresponding relative SUSY-EW and SUSY-QCD corrections δ as function of the partonic CM energy $\sqrt{\hat{s}}$ for the different SPS scenarios.

17

W-resonance region the corrections are extremely small and flat in $p_{\mathrm{T},l}$. Only extremely light gauginos with masses smaller than M_{W} could impact the precise determination of the W mass. Experimental bounds on the mass of the lightest chargino $M_{\tilde{\chi}^{\pm}} \gtrsim 100$ GeV [37] rule out such a scenario. Note that the SUSY-QCD corrections are multiplied by a factor of 10 in the plot.

The analogous results for the Tevatron are shown in Table 7 and Figure 9.

4   Conclusions

Single-W-boson production is one of the cleanest hadron collider processes and will be used to precisely determine Standard Model parameters like the W-boson mass and width. In order to match the envisaged high experimental accuracy, it is mandatory to reduce the theoretical uncertainty of the cross-section prediction to a level of one percent or better.

We have studied radiative corrections to single-W-boson production, $\mathrm{pp}/\mathrm{p}\bar{\mathrm{p}} \to \mathrm{W}^{+} \to l^{+}\nu_l X$, at the Tevatron and at the LHC. We have completed our previous calculation of the $\mathcal{O}(\alpha)$ electroweak corrections [9] by including photon–quark scattering processes. These photon-induced contributions turn out to be considerable at large lepton transverse momentum. However, they do not significantly affect the distribution in the lepton–neutrino transverse mass $M_{\mathrm{T},\nu_l l}$. We have furthermore discussed the impact of electroweak effects beyond $\mathcal{O}(\alpha)$, specifically the Sudakov logarithms which arise in the high-energy regime. The leading $\mathcal{O}(\alpha^2)$ Sudakov logarithms, which we consider as a measure for the electroweak two-loop effects, turn out to be small, below 5% even for transverse lepton momenta $p_{\mathrm{T},l}$ in the TeV range. Corrections due to multi-photon final-state radiation beyond $\mathcal{O}(\alpha)$ reach the percent level near the W resonance and distort the shape of the $p_{\mathrm{T},l}$ and $M_{\mathrm{T},\nu_l l}$ distributions. Given the high experimental accuracy envisaged specifically at the LHC, it is therefore mandatory to control the effects of multi-photon emission in the determination of the W mass.

Finally, to study the impact of new physics on the W cross section in a concrete model, we have calculated the $\mathcal{O}(\alpha)$ electroweak and $\mathcal{O}(\alpha_{\mathrm{s}})$ strong corrections to $\mathrm{pp}/\mathrm{p}\bar{\mathrm{p}} \to \mathrm{W}^{+} \to l^{+}\nu_l X$ within the MSSM. The supersymmetric corrections turn out to be negligible in the vicinity of the W resonance for viable MSSM scenarios, reaching the percent level only at very high lepton transverse momenta and for specific choices of the supersymmetric parameters. Effects from virtual SUSY particles would thus not spoil the status of single-W-boson production as one of the cleanest Standard Model candles at hadron colliders.

Acknowledgments

A   SPS benchmark scenarios

For the SPS benchmark [44] scenarios discussed in this work we use the low-energy input specified in Table 8. The input variables are the ratio t_β of the vacuum expectation values of the Higgs

	$p_{\mathrm{T},l}/\mathrm{GeV}$	25–∞	50–∞	100–∞	200–∞	500–∞	1000–∞
				$\mathrm{pp} \to l^+ \nu_l X$ at $\sqrt{s} = 14\,\mathrm{TeV}$			
SPS1a	$\delta_{\mathrm{SUSY-QCD}}/\%$	+0.0046	+0.017	+0.079	+0.29	+1.3	+0.42
SPS1a	$\delta_{\mathrm{SUSY-EW}}/\%$	−0.022	−0.077	−0.34	−0.78	−0.54	+1.2
SPS1b	$\delta_{\mathrm{SUSY-QCD}}/\%$	+0.0019	+0.0071	+0.032	+0.11	+0.60	+1.3
SPS1b	$\delta_{\mathrm{SUSY-EW}}/\%$	−0.0068	−0.028	−0.14	−0.50	−1.0	−0.20
SPS2	$\delta_{\mathrm{SUSY-QCD}}/\%$	+0.0007	+0.0026	+0.012	+0.039	+0.19	+0.71
SPS2	$\delta_{\mathrm{SUSY-EW}}/\%$	−0.061	−0.24	−0.44	+0.21	+2.3	+2.6
SPS3	$\delta_{\mathrm{SUSY-QCD}}/\%$	+0.0020	+0.0073	+0.033	+0.12	+0.62	+1.3
SPS3	$\delta_{\mathrm{SUSY-EW}}/\%$	−0.0090	−0.031	−0.15	−0.51	−1.0	−0.23
SPS4	$\delta_{\mathrm{SUSY-QCD}}/\%$	+0.0027	+0.0097	+0.044	+0.16	+0.83	+1.2
SPS4	$\delta_{\mathrm{SUSY-EW}}/\%$	−0.0095	−0.050	−0.25	−0.57	−0.44	+0.53
SPS5	$\delta_{\mathrm{SUSY-QCD}}/\%$	+0.0033	+0.012	+0.055	+0.20	+0.99	+0.89
SPS5	$\delta_{\mathrm{SUSY-EW}}/\%$	−0.016	−0.046	−0.20	−0.60	−1.2	+0.12
SPS6	$\delta_{\mathrm{SUSY-QCD}}/\%$	+0.0033	+0.012	+0.055	+0.20	+1.00	+0.88
SPS6	$\delta_{\mathrm{SUSY-EW}}/\%$	−0.013	−0.050	−0.24	−0.70	−0.70	+0.61
SPS7	$\delta_{\mathrm{SUSY-QCD}}/\%$	+0.0019	+0.0067	+0.030	+0.11	+0.57	+1.3
SPS7	$\delta_{\mathrm{SUSY-EW}}/\%$	−0.0091	−0.045	−0.23	−0.69	−0.27	+0.25
SPS8	$\delta_{\mathrm{SUSY-QCD}}/\%$	+0.0013	+0.0048	+0.022	+0.075	+0.39	+1.4
SPS8	$\delta_{\mathrm{SUSY-EW}}/\%$	−0.0067	−0.035	−0.18	−0.55	−0.30	+0.23
SPS9	$\delta_{\mathrm{SUSY-QCD}}/\%$	+0.0009	+0.0034	+0.015	+0.051	+0.26	+0.97
SPS9	$\delta_{\mathrm{SUSY-EW}}/\%$	−0.021	−0.070	−0.27	−0.10	+0.015	+0.023

Table 6: Relative SUSY-EW and SUSY-QCD corrections δ in the MSSM for W^+ production at the LHC for different ranges in $p_{\mathrm{T},l}$. The corresponding integrated LO cross sections σ_0 can be found in Table 1.

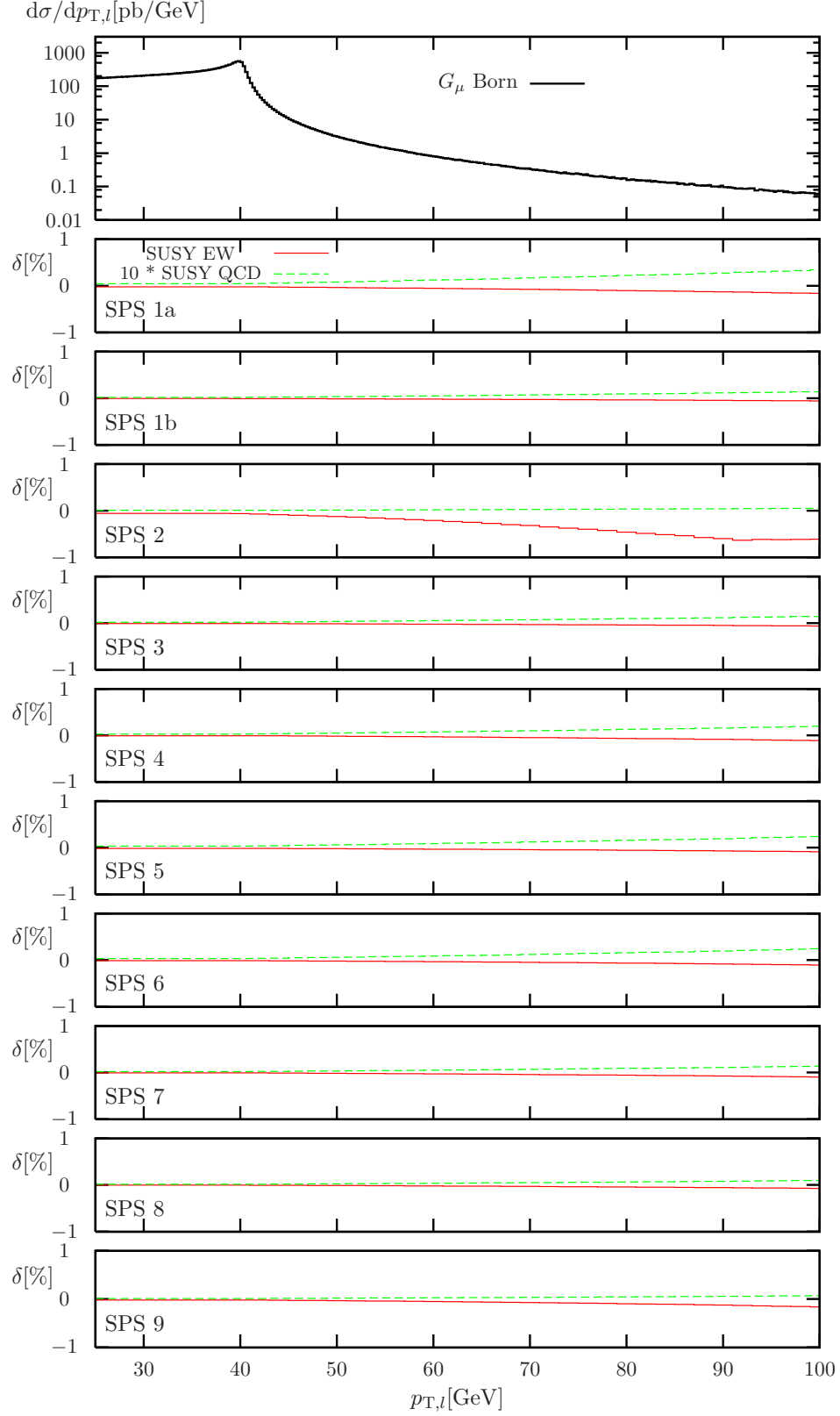**Figure 8:** Lepton-transverse-momentum distribution in LO and corresponding relative SUSY-EW and SUSY-QCD corrections δ for the different SPS scenarios at the LHC.

$$pp \to l^+\nu_l X \text{ at } \sqrt{s} = 1.96\,\text{TeV}$$

	$p_{\mathrm{T},l}/\text{GeV}$	25–∞	50–∞	75–∞	100–∞	200–∞	300–∞
SPS1a	$\delta_{\text{SUSY}-\text{QCD}}/\%$	+0.0046	+0.014	+0.032	+0.052	+0.16	+0.32
SPS1a	$\delta_{\text{SUSY}-\text{EW}}/\%$	−0.022	−0.063	−0.16	−0.27	−0.71	−0.97
SPS1b	$\delta_{\text{SUSY}-\text{QCD}}/\%$	+0.0019	+0.0057	+0.013	+0.021	+0.064	+0.12
SPS1b	$\delta_{\text{SUSY}-\text{EW}}/\%$	−0.0068	−0.022	−0.054	−0.093	−0.34	−0.69
SPS2	$\delta_{\text{SUSY}-\text{QCD}}/\%$	+0.0007	+0.0021	+0.0049	+0.0079	+0.023	+0.044
SPS2	$\delta_{\text{SUSY}-\text{EW}}/\%$	−0.061	−0.23	−0.51	−0.54	−0.15	+0.58
SPS3	$\delta_{\text{SUSY}-\text{QCD}}/\%$	+0.0020	+0.0059	+0.014	+0.022	+0.066	+0.13
SPS3	$\delta_{\text{SUSY}-\text{EW}}/\%$	−0.0089	−0.024	−0.058	−0.099	−0.35	−0.72
SPS4	$\delta_{\text{SUSY}-\text{QCD}}/\%$	+0.0026	+0.0077	+0.018	+0.029	+0.088	+0.17
SPS4	$\delta_{\text{SUSY}-\text{EW}}/\%$	−0.0094	−0.040	−0.11	−0.20	−0.61	−0.48
SPS5	$\delta_{\text{SUSY}-\text{QCD}}/\%$	+0.0032	+0.0095	+0.022	+0.036	+0.11	+0.21
SPS5	$\delta_{\text{SUSY}-\text{EW}}/\%$	−0.016	−0.037	−0.085	−0.14	−0.49	−0.69
SPS6	$\delta_{\text{SUSY}-\text{QCD}}/\%$	+0.0033	+0.0096	+0.022	+0.037	+0.11	+0.22
SPS6	$\delta_{\text{SUSY}-\text{EW}}/\%$	−0.012	−0.040	−0.10	−0.18	−0.60	−0.89
SPS7	$\delta_{\text{SUSY}-\text{QCD}}/\%$	+0.0018	+0.0054	+0.013	+0.020	+0.061	+0.12
SPS7	$\delta_{\text{SUSY}-\text{EW}}/\%$	−0.0090	−0.035	−0.094	−0.17	−0.65	−0.85
SPS8	$\delta_{\text{SUSY}-\text{QCD}}/\%$	+0.0013	+0.0039	+0.0090	+0.015	+0.043	+0.081
SPS8	$\delta_{\text{SUSY}-\text{EW}}/\%$	−0.0066	−0.027	−0.072	−0.13	−0.48	−0.65
SPS9	$\delta_{\text{SUSY}-\text{QCD}}/\%$	+0.0009	+0.0027	+0.0063	+0.010	+0.030	+0.057
SPS9	$\delta_{\text{SUSY}-\text{EW}}/\%$	−0.021	−0.060	−0.15	−0.27	−0.16	−0.048

Table 7: Relative SUSY-EW and SUSY-QCD corrections δ in the MSSM for W^+ production at the Tevatron for different ranges in $p_{\mathrm{T},l}$. The corresponding integrated LO cross sections σ_0 can be found in Table 4.
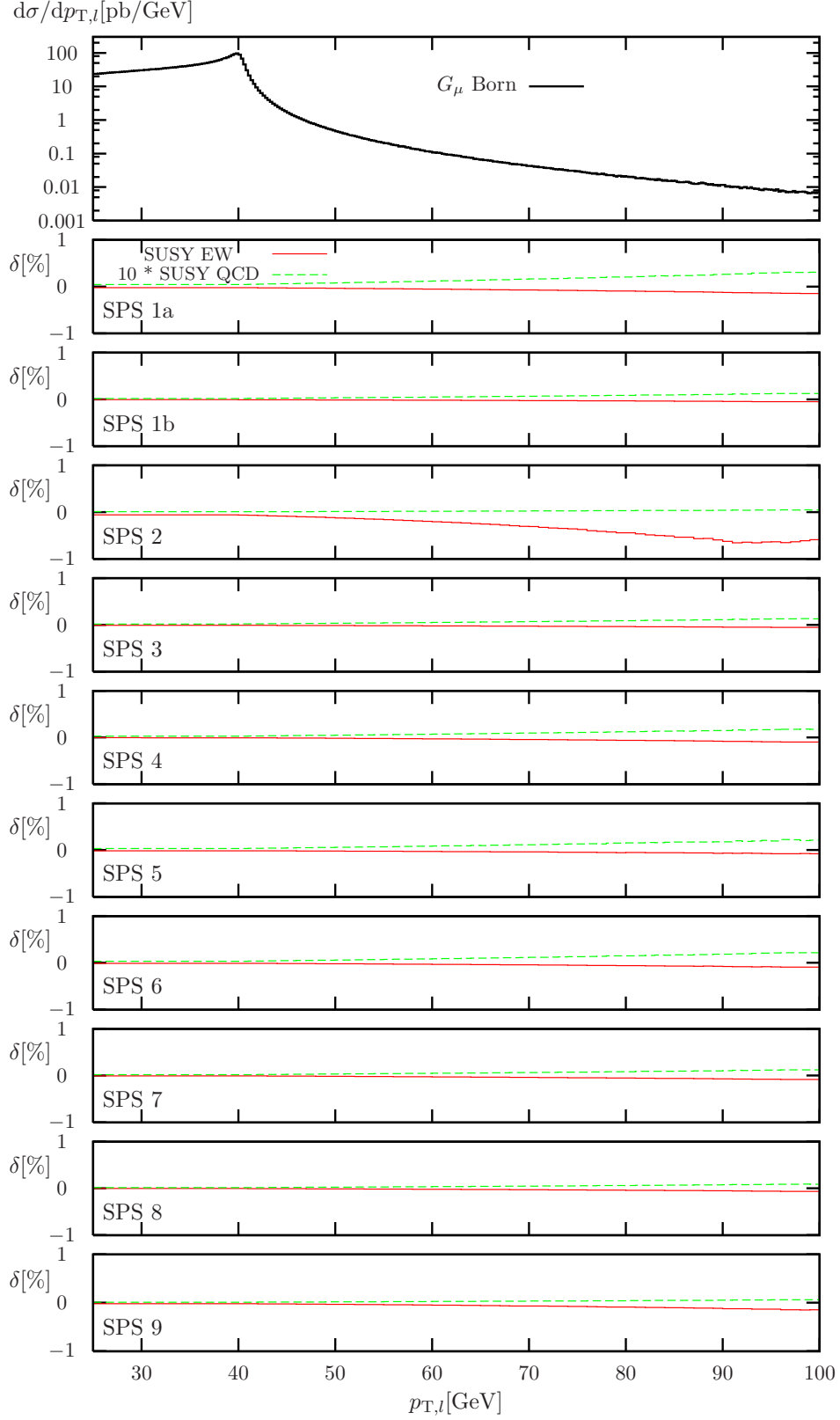
Figure 9: Lepton-transverse-momentum distribution in LO and corresponding relative SUSY-EW and SUSY-QCD corrections δ for the different SPS scenarios at the Tevatron.

bosons giving rise to up- and down-type fermion masses, the mass of the CP-odd Higgs boson, M_{A^0}, the supersymmetric Higgs mass parameter μ, the electroweak gaugino mass parameters $M_{1,2}$, the gluino mass $m_{\tilde{g}}$, the trilinear couplings $A_{\tau,\mathrm{t},\mathrm{b}}$, the scale at which the $\overline{\mathrm{DR}}$-input values are defined, $\mu_R(\overline{\mathrm{DR}})$, the soft SUSY-breaking parameters in the diagonal entries of the squark and slepton mass matrices of the first and second generations M_{fi} (where $i = L, R$ refers to the left- and right-handed sfermions, $f = q, l$ to quarks and leptons, and $f = \mathrm{u, d, e}$ to up and down quarks and electrons, respectively), and the analogous soft SUSY-breaking parameters for the third generation M_{fi}^{3G}.

Table 8: The low-energy input for the SPS scenarios. See text for details.

	SPS 1a	SPS 1b	SPS 2	SPS 3	SPS 4	SPS 5	SPS 6	SPS 7	SPS 8	SPS 9
t_β	10	30	10	10	50	5	10	15	15	10
$M_{A^0}[\text{GeV}]$	393.6	525.5	1443.0	572.4	404.4	693.9	463.0	377.9	514.5	911.7
$\mu[\text{GeV}]$	352.4	495.6	124.8	508.6	377.0	639.8	393.9	300.0	398.3	869.9
$M_1[\text{GeV}]$	99.1	162.8	120.4	162.8	120.8	121.4	195.9	168.6	140.0	-550.6
$M_2[\text{GeV}]$	192.7	310.9	234.1	311.4	233.2	234.6	232.1	326.8	271.8	-175.5
$m_{\tilde{g}}[\text{GeV}]$	595.2	916.1	784.4	914.3	721.0	710.3	708.5	926.0	820.5	1275.2
$A_\tau[\text{GeV}]$	-254.2	-195.8	-187.8	-246.1	-102.3	-1179.3	-213.4	-39.0	-36.7	1162.4
$A_t[\text{GeV}]$	-510.0	-729.3	-563.7	-733.5	-552.2	-905.6	-570.0	-319.4	-296.7	-350.3
$A_b[\text{GeV}]$	-772.7	-987.4	-797.2	-1042.2	-729.5	-1671.4	-811.3	-350.5	-330.3	216.4
$\mu_R(\overline{\text{DR}})[\text{GeV}]$	454.7	706.9	1077.1	703.8	571.3	449.8	548.3	839.6	987.8	1076.1
$M_{qL}[\text{GeV}]$	539.9	836.2	1533.6	818.3	732.2	643.9	641.3	861.3	1081.6	1219.2
$M_{dR}[\text{GeV}]$	519.5	803.9	1530.3	788.9	713.9	622.9	621.8	828.6	1029.0	1237.6
$M_{uR}[\text{GeV}]$	521.7	807.5	1530.5	792.6	716.0	625.4	629.3	831.3	1033.8	1227.9
$M_{lL}[\text{GeV}]$	196.6	334.0	1455.6	283.3	445.9	252.2	260.7	257.2	353.5	316.2
$M_{eR}[\text{GeV}]$	136.2	248.3	1451.0	173.0	414.2	186.8	232.8	119.7	170.4	300.0
$M_{qL}^{3G}[\text{GeV}]$	495.9	762.5	1295.3	760.7	640.1	535.2	591.2	836.3	1042.7	1111.6
$M_{dR}^{3G}[\text{GeV}]$	516.9	780.3	1519.9	785.6	673.4	620.5	619.0	826.9	1025.5	1231.7
$M_{uR}^{3G}[\text{GeV}]$	424.8	670.7	998.5	661.2	556.8	360.5	517.0	780.1	952.7	1003.2
$M_{lL}^{3G}[\text{GeV}]$	195.8	323.8	1449.6	282.4	394.7	250.1	259.7	256.8	352.8	307.4
$M_{eR}^{3G}[\text{GeV}]$	133.6	218.6	1438.9	170.0	289.5	180.9	230.5	117.6	167.2	281.2

References

[1] C. E. Gerber *et al.* [TeV4LHC Top and Electroweak Working Group], "Tevatron-for-LHC report: Top and electroweak physics," arXiv:0705.3251 [hep-ph].

[2] V. Büscher *et al.* [TeV4LHC Landscape Working Group], "Tevatron-for-LHC report: Preparations for discoveries," hep-ph/0608322.

[3] W. L. van Neerven and E. B. Zijlstra, Nucl. Phys. B **382** (1992) 11 [Erratum-ibid. B **680** (2004) 513];
R. V. Harlander and W. B. Kilgore, Phys. Rev. Lett. **88** (2002) 201801 [hep-ph/0201206];
C. Anastasiou, L. J. Dixon, K. Melnikov and F. Petriello, Phys. Rev. Lett. **91** (2003) 182002 [hep-ph/0306192];
C. Anastasiou, L. J. Dixon, K. Melnikov and F. Petriello, Phys. Rev. D **69** (2004) 094008 [hep-ph/0312266].

[4] V. Ravindran and J. Smith, arXiv:0708.1689 [hep-ph].

[5] S. Frixione and B. R. Webber, hep-ph/0612272.

[6] C. Balazs and C. P. Yuan, Phys. Rev. D **56** (1997) 5558 [hep-ph/9704258];
R. K. Ellis and S. Veseli, Nucl. Phys. B **511** (1998) 649 [hep-ph/9706526];
A. Kulesza and W. J. Stirling, JHEP **0001** (2000) 016 [hep-ph/9909271].

[7] S. Frixione and M. L. Mangano, JHEP **0405** (2004) 056 [hep-ph/0405130].

[8] V. A. Zykunov, Eur. Phys. J. direct C **3** (2001) 9 [hep-ph/0107059].

[9] S. Dittmaier and M. Krämer, Phys. Rev. D **65** (2002) 073007 [hep-ph/0109062].

[10] U. Baur and D. Wackeroth, Phys. Rev. D **70** (2004) 073015 [hep-ph/0405191];
A. Arbuzov, D. Bardin, S. Bondarenko, P. Christova, L. Kalinovskaya, G. Nanava and R. Sadykov, Eur. Phys. J. C **46** (2006) 407 [Erratum-ibid. C **50** (2007) 505] [hep-ph/0506110].

[11] C. M. Carloni Calame, G. Montagna, O. Nicrosini and A. Vicini, JHEP **0612** (2006) 016 [hep-ph/0609170].

[12] C. Buttar *et al.*, "Les Houches physics at TeV colliders 2005, standard model, QCD, EW, and Higgs working group: Summary report," hep-ph/0604120.

[13] S. Dittmaier and M. Krämer, in Ref. [12].

[14] A. B. Arbuzov and R. R. Sadykov, arXiv:0707.0423 [hep-ph].

[15] C. M. Carloni Calame, G. Montagna, O. Nicrosini and M. Treccani, Phys. Rev. D **69** (2004) 037301 [hep-ph/0303102].

[16] W. Placzek and S. Jadach, Eur. Phys. J. C **29** (2003) 325 [hep-ph/0302065];
C. M. Carloni Calame, S. Jadach, G. Montagna, O. Nicrosini and W. Placzek, Acta Phys. Polon. B **35** (2004) 1643 [hep-ph/0402235].

[17] Q. H. Cao and C. P. Yuan, Phys. Rev. Lett. **93** (2004) 042001 [hep-ph/0401026];
B. F. L. Ward, C. Glosser, S. Jadach and S. A. Yost, Int. J. Mod. Phys. A **20** (2005) 3735 [hep-ph/0411047];
B. F. L. Ward and S. A. Yost, Acta Phys. Polon. B **38** (2007) 2395 [arXiv:0704.0294 [hep-ph]];
G. Montagna, talk given at "Loopfest IV: Radiative Corrections for the LHC and ILC", Fermilab, 2007.

[18] J. H. Kühn, A. Kulesza, S. Pozzorini and M. Schulze, Phys. Lett. B **651** (2007) 160 [hep-ph/0703283] and arXiv:0708.0476 [hep-ph];
W. Hollik, T. Kasprzik and B. A. Kniehl, arXiv:0707.2553 [hep-ph].

[19] G. J. Gounaris, J. Layssac and F. M. Renard, arXiv:0709.1789 [hep-ph].

[20] S. Dittmaier, Nucl. Phys. B **565** (2000) 69 [hep-ph/9904440].

[21] S. Dittmaier and T. Kasprzik, in preparation. For pure final-state radiation the extension of the dipole subtraction has already been described in Ref. [22].

[22] A. Bredenstein, S. Dittmaier and M. Roth, Eur. Phys. J. C **44** (2005) 27 [hep-ph/0506005].

[23] M. Consoli, W. Hollik and F. Jegerlehner, Phys. Lett. B **227** (1989) 167.

[24] K. P. Diener, S. Dittmaier and W. Hollik, Phys. Rev. D **72** (2005) 093002 [hep-ph/0509084].

[25] V. S. Fadin, L. N. Lipatov, A. D. Martin and M. Melles, Phys. Rev. D **61** (2000) 094002 [hep-ph/9910338].

[26] M. Ciafaloni, P. Ciafaloni and D. Comelli, Phys. Rev. Lett. **84** (2000) 4810 [hep-ph/0001142].

[27] M. Hori, H. Kawamura and J. Kodaira, Phys. Lett. B **491** (2000) 275 [hep-ph/0007329].

[28] M. Melles, Eur. Phys. J. C **24** (2002) 193 [hep-ph/0108221].

[29] W. Beenakker and A. Werthenbach, Nucl. Phys. B **630** (2002) 3 [hep-ph/0112030].

[30] A. Denner, M. Melles and S. Pozzorini, Nucl. Phys. B **662** (2003) 299 [hep-ph/0301241].

[31] B. Jantzen, J. H. Kühn, A. A. Penin and V. A. Smirnov, Phys. Rev. D **72** (2005) 051301 [Erratum-ibid. D **74** (2006) 019901] [hep-ph/0504111] and Nucl. Phys. B **731** (2005) 188 [Erratum-ibid. B **752** (2006) 327] [hep-ph/0509157].

[32] A. Denner, B. Jantzen and S. Pozzorini, Nucl. Phys. B **761** (2007) 1 [hep-ph/0608326].

[33] P. Ciafaloni and D. Comelli, JHEP **0609** (2006) 055 [hep-ph/0604070];
U. Baur, Phys. Rev. D **75** (2007) 013005 [hep-ph/0611241].

[34] A. D. Martin, R. G. Roberts, W. J. Stirling and R. S. Thorne, Eur. Phys. J. C **39** (2005) 155 [hep-ph/0411040].

[35] T. Kinoshita, J. Math. Phys. **3** (1962) 650;
T. D. Lee and M. Nauenberg, Phys. Rev. **133** (1964) B1549.

[36] E. A. Kuraev and V. S. Fadin, Sov. J. Nucl. Phys. **41** (1985) 466 [Yad. Fiz. **41** (1985) 733];
G. Altarelli and G. Martinelli, *In Ellis, J. (Ed.), Peccei, R.d. (Ed.): Physics At Lep, Vol. 1, 47-57;*
O. Nicrosini and L. Trentadue, Phys. Lett. B **196** (1987) 551;
O. Nicrosini and L. Trentadue, Z. Phys. C **39** (1988) 479;
F. A. Berends, W. L. van Neerven and G. J. H. Burgers, Nucl. Phys. B **297** (1988) 429 [Erratum-ibid. B **304** (1988) 921];
A. B. Arbuzov, Phys. Lett. B **470** (1999) 252 [hep-ph/9908361].

[37] W. M. Yao *et al.* [Particle Data Group], J. Phys. G **33** (2006) 1.

[38] F. Jegerlehner, DESY 01-029, LC-TH-2001-035 [hep-ph/0105283].

[39] V. M. Abazov *et al.* [CDF Collaboration], Phys. Rev. D **70** (2004) 092008 [hep-ex/0311039].

[40] J. Campbell and R. K. Ellis, MCFM – Monte Carlo for FeMtobarn processes, `http://mcfm.fnal.gov/`.

[41] J. Smith, W. L. van Neerven and J. A. M. Vermaseren, Phys. Rev. Lett. **50** (1983) 1738.

[42] T. Hahn, Comput. Phys. Commun. **140** (2001) 418 [hep-ph/0012260];
T. Hahn and C. Schappacher, Comput. Phys. Commun. **143** (2002) 54 [hep-ph/0105349].

[43] T. Hahn and M. Perez-Victoria, Comput. Phys. Commun. **118** (1999) 153 [hep-ph/9807565].

[44] B. C. Allanach *et al.*, Eur. Phys. J. C **25** (2002) 113 [eConf **C010630** (2001) P125] [hep-ph/0202233].

[45] see: `http://www.cpt.dur.ac.uk/~georg/sps/`